

Cell nuclei image segmentation using U-Net and DeepLabV3+ with transfer learning and regularization

Dina Koishiyeva¹, Madina Sydybayeva¹, Saule Belginova², Damelya Yeskendirova³,
Zhanerke Azamatova⁴, Azamat Kalpebayev¹, Gulzhanat Beketova¹

¹Almaty University of Power Engineering and Telecommunications named after G. Daukeyev, Almaty, Kazakhstan

²Department of Information Technology, University "Turan", Almaty, Kazakhstan

³International University of Information Technologies, Almaty, Kazakhstan

⁴East Kazakhstan State Technical University named after D.Serikbayev, Oskemen, Kazakhstan

Article Info

Article history:

Received Mar 16, 2024

Revised May 7, 2024

Accepted May 12, 2024

Keywords:

DeeplabV3plus

Nuclei segmentation

Regularization

Transfer learning

U-Net

ABSTRACT

Semantic nuclei segmentation is a challenging area of computer vision. Accurate nuclei segmentation can help medics in diagnosing many diseases. Automatic nuclei segmentation can help medics in diagnosing many diseases such as cancer by providing automatic tissue analysis. Deep learning algorithms allow automatic feature extraction from medical images, however, hematoxylin and eosin (H&E) stained images are challenging due to variability in staining and textures. Using pre-trained models in deep learning speeds up development and improves their performance. This paper compares Deeplabv3+ and U-Net deep learning methods with the pre-trained models ResNet-50 and EfficientNetB4 embedded in their architecture. In addition, different regularization and dropout parameters are applied to prevent overtraining. The experiment was conducted on the PanNuke dataset consisting of nearly 8,000 histological images and annotated nuclei. As a result, the ResNet50-based DeepLabV3+ model with L2 regularization of 0.02 and dropout of 0.7 showed efficiency with dice coefficient (DCS) of 0.8356, intersection over union (IOU) of 0.7280, and loss of 0.3212 on the test set.

This is an open access article under the [CC BY-SA](https://creativecommons.org/licenses/by-sa/4.0/) license.



Corresponding Author:

Saule Belginova

Department of Information Technology, University "Turan"

Almaty, Kazakhstan

Email: sbelginova@gmail.com

1. INTRODUCTION

Medical image segmentation is a traditionally challenging area of research in computer vision. For many years now, nuclei segmentation on histological images has been a current area of research. The size of the cell nucleus is key to cancer diagnosis, as changes in its size and shape often indicate malignant cell transformation [1]. Globally, cancer remains a major cause of death, with millions of new cases and deaths registered every year [2]. In the Republic of Kazakhstan, the cancer incidence rate is steadily increasing, indicating a growing public health problem [3]. Segmenting the area and mapping the contours of the nuclei on histological images can help to reduce statistics in early diagnosis. There are traditional segmentation methods, such as manual segmentation, where an expert manually highlights areas of interest on images, but this method can be time-consuming, especially with large amounts of data [4]. It can also include thresholding and clustering methods, including K-means-based methods [5], which automate the process of structure extraction, but these methods can also face difficulties in separating overlapping or closely spaced objects [6]. Hematoxylin and eosin staining (H&E) is used to highlight nuclear and cytoplasmic structures in

tissues, where hematoxylin stains the nuclei blue and eosin stains the cytoplasm pink [7]. Tissue slices are then digitized using scanners, turning them into digital images. The complexity of digital histological images is due to variability in staining, patterns, density and overlap of cellular structures, presence of artifacts, and high-resolution images [8]. To analyze and segment objects of interest, advanced architectures are needed. Recently, there have been many developments in deep learning, namely convolutional neural networks (CNNs) for visual analysis. CNNs are characterized by the depth and available convolution kernels and greater adaptability [9]. However, they also have the disadvantages of having a large amount of partitioned data, can also encounter difficulties in generalizing to real data, and requiring tuning of filter sizes and more computational resources [10]. To overcome some of the limitations of CNNs, pre-trained models on big data can be introduced into the main convolutional layers, this can help to speed up the learning process and transfer already extracted features and knowledge to new tasks, reducing the need for large amounts of data [11], [12]. Complex architectures with a large number of parameters and filters, often face overtraining problems, when a model is not able to analyze unfamiliar images well [13]. To overcome overtraining, CNNs use regularization methods such as dropout, which eliminates random neurons during training to increase the generalizability of the model. Other methods, including regularization, add penalties for large weights, increasing stability and reducing dependence on noise in the data [14]. In our study, this experiment was performed on an extensive dataset for nuclei segmentation on H&E images, where noise and intensity analysis of regions of interest was performed, we also compared the performance of the deep learning model with pre-trained deep learning models and adapted regularization parameters. The main contributions and innovations of this paper are as follows:

- Development and comparison of deep learning methods for cell nuclei segmentation: our work contributes to the field of automatic nuclei segmentation of cell nuclei by comparing the performance of two advanced deep learning methods, DeepLabV3+ and U-Net, with the inclusion of pre-trained models ResNet-50 and EfficientNetB4.
- Applying transfer learning and regularization to improve performance: to prevent overtraining, different regularization methods were applied to the four learned models.
- Experimental study on the PanNuke dataset: an experiment was conducted on the extensive PanNuke dataset containing about 8,000 histological images, with a variety of staining and nuclei sizes.

This study offers insights into optimizing cell nuclei segmentation methods, which could improve automated analysis of histological images and help medical professionals in the diagnosis of cancer and other diseases. The raw data for the study were taken from an open source on Kaggle: cancer institutional segmentation and classification dataset. All materials related to model code and training are available upon request to support transparency and validation of our results.

2. LITERATURE REVIEW

This section presents research on nuclei segmentation on H&E stained images. Many methods have been developed, but despite significant advances in medical imaging, the problem of accurate and efficient nuclei segmentation remains relevant. The complexity of the task is due to the high degree of variability in the staining, shape, and size of nuclei from different organs, as well as the presence of overlapping structures and artifacts in tissue samples [15], [16]. Deep neural networks (DNNs) especially CNNs show better results in contrast to traditional image processing algorithms [17]. Currently, there are many methods based on CNNs, they differ in architecture, encoder and decoder layer configuration, and additional blocks.

The U-Net [18] model developed specifically for bio-medical segmentation tasks is characterized by a symmetric architecture, also the presence of skip connections, to transfer features between the encoder and decoder directly, it has shown good results, especially on small datasets, however, it has disadvantages in limited perception of the global context of the image [19]. Many developments and modifications of the classical U-Net exist, additional blocks of attention [20], residuals are introduced, and other multiscale approaches [21]. The paper by Li *et al.* [22] presents a novel dual U-Net architecture aimed at addressing the complex challenge of nucleus segmentation in gliomas, the model uses a dual upsampling path structure combining a classification model for boundary segmentation and a regression model for distance map prediction, according to the results F1-score is 0.82 and Jaccard index is 0.66. The MIU-Net model developed for nuclei segmentation of histological images, by Li and Li [23], includes modified nucleation modules and attention mechanisms, with AUC results of 0.92. DCSA-Net model for cell nuclei segmentation on histopathological images by Sumon *et al.* [24] it uses a combination of convolutional and spatial attention mechanisms, with results accuracy of 96.4%, and dice 73.2%. Besides skip-connection-based models, other architectures for semantic nuclei segmentation have been developed. The NucleiSegNet model of Lal, Shyam, et al. proposes an architecture for deep nuclei segmentation in liver cancer histopathological images, the architecture includes a robust residual block, a bottleneck block, and an attention decoder block [25].

Model CIA-Net by Zhou *et al.* [26] for segmenting nuclei instances in pathology images, this network leverages spatial and texture relationships between nuclei and contours, enhancing accuracy and robustness. CNNs architectures use pre-trained weights to carry learned semantic cues in addition to the underlying models, improving performance [27].

Efficient U-Net++ [28], a model combining U-Net++ [29] with the EfficientNet backbone, it utilizes pre-trained EfficientNet from B0 to B5 trained on ImageNet [30] the model's decoder block links to the EfficientNet encoder through nested dense convolutional blocks. The WBC-Net model [31], based on U-Net++ and ResNet [32], is intended for leukocyte cell segmentation, it includes a context-aware feature coder with residual blocks and mixed skip paths on dense convolutional blocks for feature association. In addition to ResNet and EfficientNet, other architectures such as inception [33], DenseNet [34], and VGG are being integrated into complex CNNs [35] frameworks to improve performance. Complex models, enhanced by combining architectures and adding layers, risk overfitting, to counter this, data augmentation diversifies training data [36], regularization penalizes complexity, and dropout reduces dependency on specific neuron pathways, aiding generalization [37]. In summary, the choice of a model for nuclei segmentation depends on a balance between complexity and efficiency, taking into account staining variability, image resolution, and the need for accurate contouring, which can assist clinicians in the diagnosis of multiple diseases.

3. METHODS AND MATERIALS

In this study, experiments were conducted using four deep models, namely U-Net with pre-trained ResNet-50 [38], U-Net with EfficientNetB4 [39] and DeeplabV3+ with transfer ResNet-50 [40] also DeeplabV3+ with EfficientNetB4 [41]. This section describes all the technical details of the implementation of the models. This section describes the technical specifications of the models, along with the differences in implementation.

3.1. U-Net with ResNet-50 (U-Net ResNet50)

The U-Net architecture with ResNet-50 as an encoder combines the advantages of both models to create a new architecture for image segmentation tasks. U-Net is characterized by an encoder-decoder structure with missing links, while ResNet-50, trained on the ImageNet dataset [42], implements short links that are either identity mappings or projective short links, using 1×1 convolutions for size matching, which are particularly effective for size scaling. The integration of ResNet-50, a deep CNN with residual learning, improves the encoding part of U-Net. The study modified the model by adding additional convolutional blocks, which is a double convolutional layer with batch-normalization [43] and ReLU activation [44]. L2 regularization is implemented in all convolutional layers with a factor of 0.01 [45]. Dropout was integrated into the model as well to prevent neuronal co-adaptation, applying it with different intensities in different parts of the model [46]. In the convolutional block, a dropout rate of 0.2 is used, which means that 20% of neurons are excluded at each training step, promoting diversity in learning and reducing the risk of overtraining. In deeper layers of the decoder, the dropout rate is increased to 0.5.

3.2 U-Net with efficientNetB4 (U-Net eff4)

The U-Net ResNet50 model is a modified version of U-Net integrated with the EfficientNetB4 convolutional network. This model includes convolutional blocks that contain a pair of convolutional layers with L2 regularization and an intermediate dropout set at 0.25 to reduce overtraining. Batch-normalization and ReLU activation operations following the convolutional layers help to improve the nonlinearity of the data representation, shown in Figure 1. Max-pooling compressive blocks reduce dimensionality, increasing abstraction and reducing computational requirements, while expanding blocks including transposed convolution and concatenation operations provide detailed image reconstruction. Figure 2 displays the overall architecture of U-Net with a pre-trained backbone.

3.3 DeepLabV3+ with ResNet-50 (DLV3+ResNet50)

The study utilizes a modified DeepLabV3+ architecture for semantic image segmentation using the atrous spatial pyramid pooling (ASPP) approach combined with a pre-trained ResNet50 network [47]. In the ASPP block used in the architecture, the main input data passes through four parallel processing paths. The first path involves averaging pooling, which compresses the input image to a single representation, then applies 1×1 convolution to extract features, shown in Figure 3, reconstructed to the original image size using bilinear upsampling. The remaining three paths contain 3×3 atrous convolutions with sparsity ratios that allow the network to process features at different spatial scales, each with batch normalization and ReLU activation.

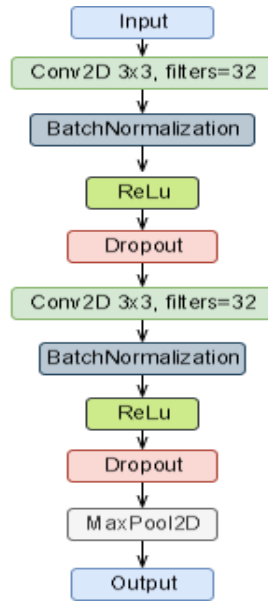


Figure 1. Contracting block

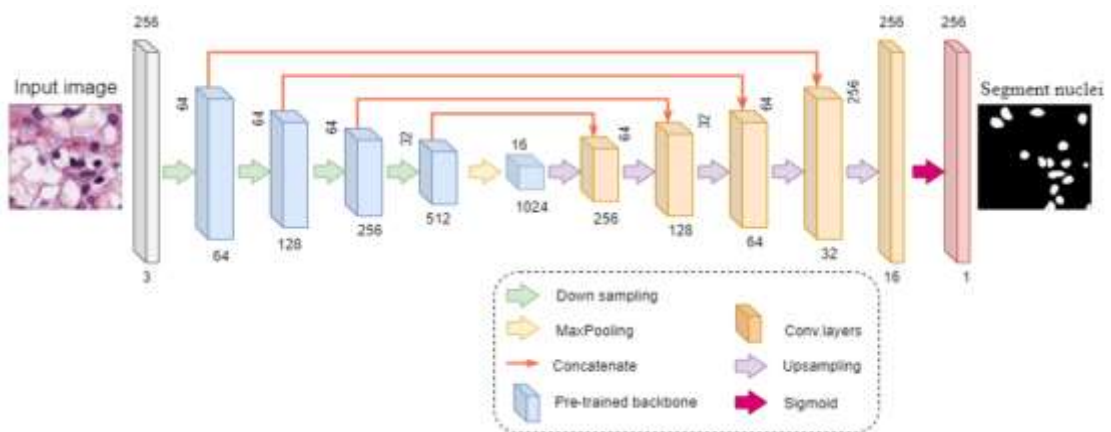


Figure 2. U-Net architecture with pre-trained backbone

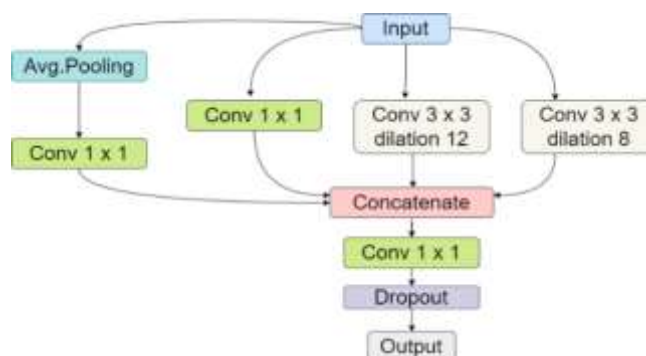


Figure 3. ASPP block

3.4. DeepLabV3+ with EfficientNetB4 (DLV3+ Eff4)

The DLV3+ Eff4 model is a modification of the DeepLabV3+ architecture in which the ASPP block is also a key element, allowing the network to handle multi-scale information adaptively. We added two

additional convolutional layers to the model, introducing L2 regularization and dropout to prevent overtraining. The pre-trained EfficientNetB4 baseline model serves as the basis for feature extraction, applying scaling mechanisms to optimize network depth and resolution. The extracted features from the EfficientNetB4 intermediate layers are fed into ASPP and subsequent convolutional and upsampling layers. Figure 4 illustrates the overall architecture of DeepLabV3+ with a pre-trained backbone. Then in the following section, the differences in parameters and the remaining characteristics of the models will be summarized.

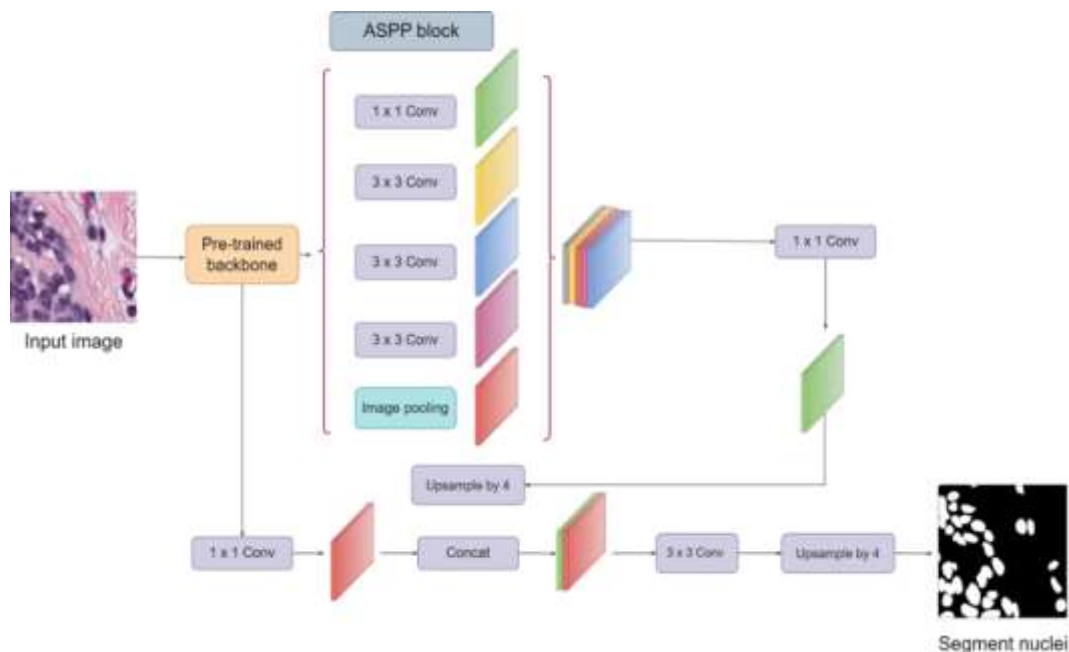


Figure 4. DeepLabV3+ architecture with pre-trained backbone

3.5. Comparison of parameters of deep learning models

The section compares four deep learning model architectures used in the research experiment for nuclei segmentation, based on different methods, dropout degree, convolution kernels used, L2 regularization coefficients, basis networks, and total number of parameters. The analyses are described in Table 1. In the research experiment for nuclei segmentation, additional convolution layers were introduced in U-Net and DeepLabV3+ models based on different underlying networks ResNet50 and EfficientNetB4 with different parameters also dropout and L2-regularisation parameters were introduced. The choice of dropout and L2-regularisation values for the models was done to balance feature extraction power and robustness to overfitting, taking into account the architecture and parameters of each network. In contrast, models integrated with EfficientNetB4, assuming a more efficient use of parameters, allow a lower dropout level, to 0.25 for DeepLabV3 and the application of a more lenient L2-regularisation (0.01), promoting the preservation of important traits while reducing the risk of overtraining.

Table 1. Comparison of model architectures with different parameters and methods

Model	Method	Dropout	Kernel	L2	Backbone	Parameters (M)	Size (MB)
U-Net ResNet50	Conv, Transpose	0.7	3*3	0.01	ResNet50	15.676.865	59.80
U-Net eff4	Conv, Transpose	0.5	3*3	0.01	EfficientNetB4	14.932.072	56.96
DLV3+ ResNet50	ASPP	0.7	3*3	0.02	ResNet50	30.462.849	116.21
DLV3+ eff4	ASPP	0.25	3*3	0.01	EfficientNetB4	14.306.600	54.58

3.6. Dataset description

Dataset with nuclei PanNuke [48] is a set of 7,901 masked images designed for nuclei segmentation and classification on slides of cancer-affected tissue images. It includes about 200,000 annotated nuclei. The dataset has been semi-automatically annotated and has undergone quality control by clinical experts to

create data that approximates real-world clinical conditions. Figure 5 shows some sample images and annotated masks from the dataset. As shown in examples from the PanNuke dataset, the images demonstrate the diversity of nuclei shapes and sizes in cancer tissues. This highlights the complexity of the conditions that models must cope with when analyzing cancer tissues.

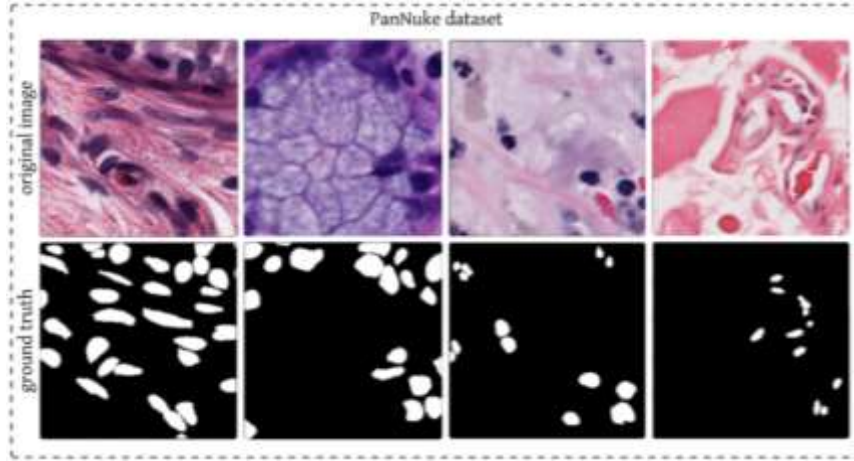


Figure 5. Several sample images and masks from the PanNuke dataset

3.7. Evaluation assessment metrics

In this research work, four metrics namely dice coefficient (DCS), intersection over union (IOU), accuracy (Acc), and dice loss (Loss) are used to evaluate the performance of deep CNNs [49]. According to the equation, it is used to calculate the shift of the center of change along the image axis. DCS is the rate of overlap between the prediction and the given binary labels calculated using an equation. IoU metric calculated by equation. Acc metric is the exact classification of each pixel is calculated using equation [50]. Dice loss further referred to hereafter as loss was chosen as the loss function instead of binary cross-entropy because it is effective in tasks with non-uniform class distribution, typical of medical segmentation, where exact matching of predicted masks with real masks is important [51].

$$DCS = \frac{2TP}{TP+FP+FN} \tag{1}$$

$$IoU = \frac{TP}{TP+FP+FN} \tag{2}$$

$$Acc = \frac{TP+TN}{TP+FP+FN+TN} \tag{3}$$

$$Loss = 1 - \sum_{k=0}^k \frac{2w_k \sum_i^N p(k^n,i)g(k^n,i)}{\sum_i^N p^2(k^n,i)+g^2[(k^n,i)]} \tag{4}$$

Where DCS is calculated as twice the intersection of predicted and true positives (TP) divided by the sum of TP, false positives (FP), and false negatives (FN). IOU is calculated as the ratio of the intersection of TP to the union of these areas (TP, FP, and FN) [52]. Acc is an overall measure of classification correctness, which is calculated as the proportion of correctly classified cases (TP and true negative TN) out of all cases (TP, TN, FP, and FN). Also, loss is a weighted sum that takes into account the probabilities (p) of the model predictions and the true values (g), with a weight of w_i equal to class i . These metrics are necessary to evaluate the performance of neural networks.

3.8. Technical and software implementation details

The Google Colab [53] collaboration environment provided the necessary infrastructure for code execution and model training. The computational experiments in the study were performed on an NVIDIA tesla V100 GPU, which has 5,120 CUDA cores, 640 tensor cores and is equipped with 16/32 GB of HBM2 memory to efficiently process complex machine learning tasks [54]. The study used Python version 3.10.12 for scripting and data manipulation, and TensorFlow version 2.15.0 for implementing and training neural network models [55].

4. RESULTS AND DISCUSSION

The study results are presented as tables showing the mean values and standard deviation for the metrics and models on the training and validation data. Results from the test set are also presented, results have been rounded to four decimal places. The batch size is 8, the optimizer is Adam, and the learning rate for each set was adjusted dynamically depending on the iteration results and the number of epochs, with an initial value of $1e-4$, which is 0.0001. The PanNuke dataset, consisting of 7,901 images and annotated masks, was divided into training 4,297 images, validation 1,075 images, and test 1,344 image sets. The masks were transformed so that the pixel values were 0.1 and the images were scaled so that the pixel values ranged from 0 to 255. The number of epochs was set to 120. Table 2 shows the results of the training set.

On the training dataset, the U-Net ResNet50 and DLV3+ ResNet50 models show similar DCS of 0.89 ± 0.06 , SN of 0.93 ± 0.03 , and IOU of 0.87 ± 0.05 , but U-Net ResNet50 has high accuracy of 0.98 ± 0.01 and lower loss of 0.16 ± 0.88 . It is important to note that despite the higher standard deviation in the error value, the DLV3+ ResNet50 model maintains competitive DCS and IOU performance, which may indicate its robustness to different data conditions. On the other hand, the U-Net eff4 model, despite its slightly higher error value, shows stable performance in all metrics, which may provide reliable segmentation in practical applications. Following Figures 6-10 are plots of the DCS, IOU, and Acc metrics.

The U-Net eff4 model has a similar DCS of 0.89 ± 0.06 and accuracy of 0.97 ± 0.01 with DLV3+ ResNet50, but a lower IOU of 0.85 ± 0.06 . On the other hand, the DLV3+ eff4 model has an accuracy of 0.98 ± 0.01 and a low loss of 0.06 ± 0.19 , but performance is lower than the other models where DCS 0.87 ± 0.04 and IOU 0.83 ± 0.05 . Table 3 shows the results from the validation set.

On the validation dataset, U-Net ResNet50 and U-Net eff4 models showed similar DCS values around 0.80 ± 0.05 and slightly higher accuracy 0.94 ± 0.01 compared to the other models. However, U-Net eff4 slightly outperformed U-Net ResNet50 in SN value and IOU, reaching 0.83 ± 0.05 and 0.81 ± 0.05 , compared to 0.81 ± 0.07 and 0.81 ± 0.05 for U-Net ResNet50.

DLV3+ ResNet50 had a slightly higher loss 0.26 ± 0.08 and lower DCS 0.81 ± 0.05 compared to U-Net models. However, this model had a lower IOU of 0.71 ± 0.01 . DLV3+eff4 showed a lower loss at 0.25 ± 0.31 and comparable accuracy of 0.94 ± 0.01 compared to DLV3+ResNet50, but had the lowest DCS at 0.75 ± 0.08 and the lowest IOU at 0.68 ± 0.05 . Further Table 4 shows the results of the test set consisting of 1,344 images and annotated masks

Table 2. Performance evaluation on the training set (mean \pm standard deviation)

Model	Loss	Acc	DCS	SN	IOU
U-Net ResNet50	0.16 ± 0.88	0.98 ± 0.01	0.89 ± 0.06	0.93 ± 0.03	0.87 ± 0.05
U-Net eff4	0.12 ± 0.48	0.97 ± 0.01	0.89 ± 0.06	0.92 ± 0.03	0.85 ± 0.06
DLV3+ ResNet50	0.25 ± 1.66	0.97 ± 0.01	0.89 ± 0.06	0.94 ± 0.03	0.90 ± 0.05
DLV3+ eff4	0.06 ± 0.19	0.98 ± 0.01	0.87 ± 0.04	0.91 ± 0.03	0.83 ± 0.05

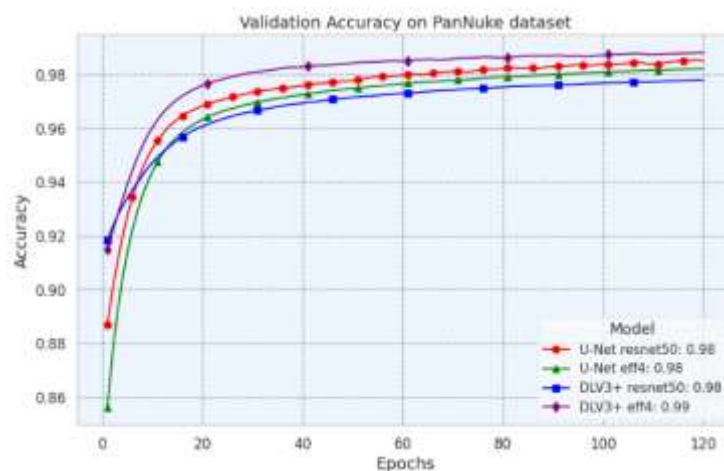


Figure 6. Dynamics of Acc

The performance of four models, U-Net ResNet50, U-Net eff4, DLV3+ResNet50, and DLV3+ eff4 were evaluated on the test dataset. The DLV3+ ResNet50 model showed the highest values of DCS of 0.8356

IOU of 0.7280, and accuracy of 0.9455. The U-Net ResNet50 and U-Net eff4 models showed similar DCS and IOU values of 0.8286 and 0.8116 for U-Net ResNet50, and 0.8138 and 0.7911 for U-Net eff4 and accuracy of 0.9474 and 0.9458. On the other hand, the DLV3+eff4 model showed the lowest DCS values of 0.6419 and IOU of 0.4893 and a lower accuracy of 0.9166. Table 5 shows the results of training time and average model output time.

According to the results of learning time and inference, the U-Net ResNet50 model has an average inference time of about 0.93 seconds and a learning time of about 37.42 minutes. The U-Net eff4 model shows an average inference time of about 0.88 seconds and a longer training time of about 43.65 minutes. On the other hand, DLV3+ResNet50 has a faster average inference time of about 0.50 seconds and a learning time of about 23.37 minutes, while DLV3+ eff4 shows an average inference time of about 0.64 seconds and a learning time of about 34.41 minutes. Based on this information, the DLV3+ResNet50 model provides a relatively faster inference time and shorter learning time compared to the other models, making it an advantageous option for implementation. Figure 11 shows a comparison of the original images, the annotated masks created by the experts, and the segmentation results generated by the four models. The model predictions are expressed in three colors, where blue indicates correct objects, red indicates model errors, and green indicates missing areas.

Table 3. Performance evaluation on the validation set (mean ± standard deviation)

Model	Loss	Acc	DCS	SN	IOU
U-Net ResNet50	0.30 ±0.25	0.94 ±0.01	0.80 ±0.05	0.81 ±0.07	0.81 ±0.05
U-Net eff4	0.22 ±0.16	0.95 ±0.01	0.80 ±0.05	0.83 ±0.05	0.81 ±0.05
DLV3+ ResNet50	0.26 ±0.08	0.94 ±0.00	0.81 ±0.05	0.81 ±0.09	0.71 ±0.01
DLV3+ eff4	0.25 ±0.31	0.94 ±0.01	0.75 ±0.08	0.83 ±0.03	0.68 ±0.05

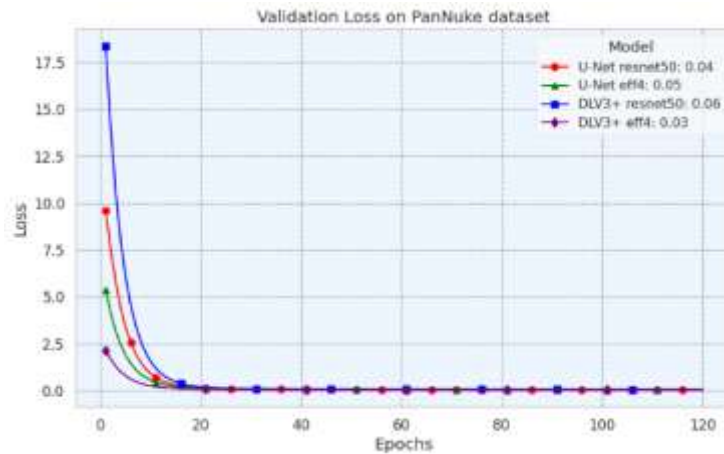


Figure 7. Dynamics of loss

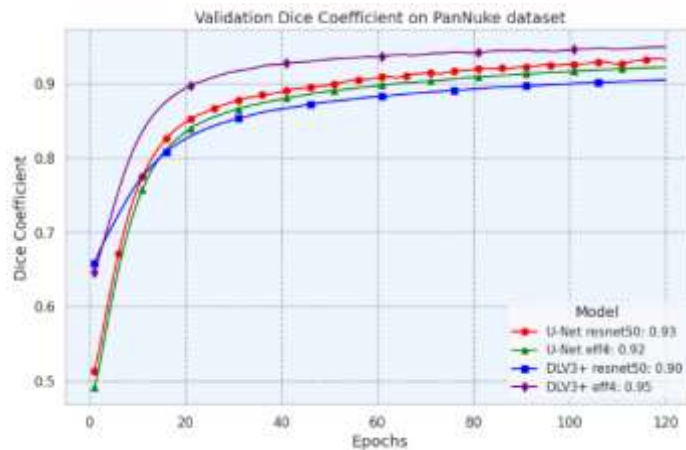


Figure 8. Dynamics of DCS

Table 4. Performance evaluation on the validation set (mean ± standard deviation)

Model	Loss	Acc	DCS	SN	IOU
U-Net ResNet50	0.3272	0.9474	0.8286	0.8116	0.7121
U-Net eff4	0.2827	0.9458	0.8138	0.7911	0.7111
DLV3+ ResNet50	0.3212	0.9455	0.8356	0.8570	0.7280
DLV3+ eff4	0.3543	0.9166	0.6419	0.5212	0.4893

Table 5. Model training and inference time

Model	Inference time (s)	Training time (min)
U-Net ResNet50	0.3272	0.9474
U-Net eff4	0.2827	0.9458
DLV3+ ResNet50	0.3212	0.9455
DLV3+ eff4	0.3543	0.9166

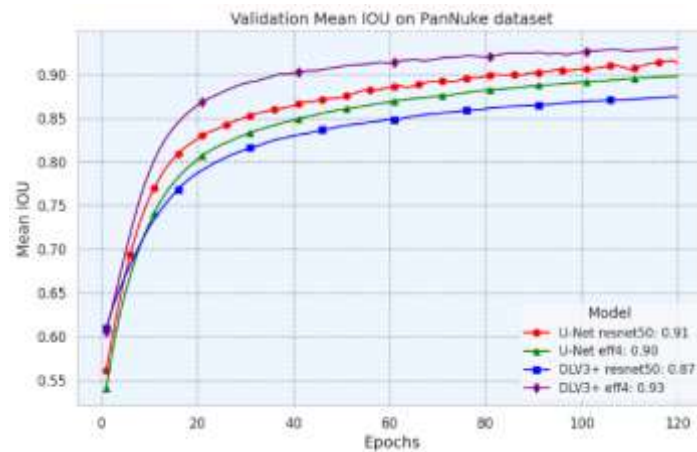


Figure 9. Dynamics of IoU

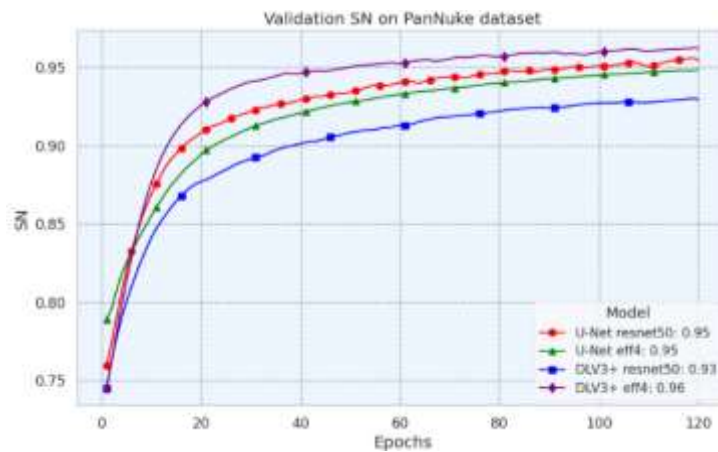


Figure 10. Dynamics of SN

Further in Figure 12, several examples are displayed prediction contours are plotted on the images to compare the four models. This visualization method, shown in Figure 12, allows a direct comparison of how closely the predicted boundaries of each model match the actual contours of the cell nuclei. Together, Figures 11 and 12 provide a complete visual assessment of the model’s performance in cell nuclei segmentation. It is possible to create a system based on a DNN that displays nuclei segments and separately visualizes nuclei contours in the image.

Figures 13-15 are plots of the DCS, IOU, and Acc metrics to visually compare the models across the three dataset sets, in percentages. These graphs enable a straightforward evaluation of each model’s

performance metrics. They help highlight the strengths and weaknesses of the models across different conditions and dataset variations.

DLV3+ ResNet50 leads the performance with a DCS of 83.56% on the test set, showing its advantage over the others. U-Net ResNet50 and U-Net eff4 remain competitive in all phases, their performance is close or slightly behind, in particular 82.86% and 81.38% respectively on the test set. DLV3+ eff4, having started with 87% in training, falls to 64.19% in the test, showing a decline. This decline for DLV3+ eff4 suggests that it may be overfitting the training data, as evidenced by its high performance in training relative to its significantly lower test results.

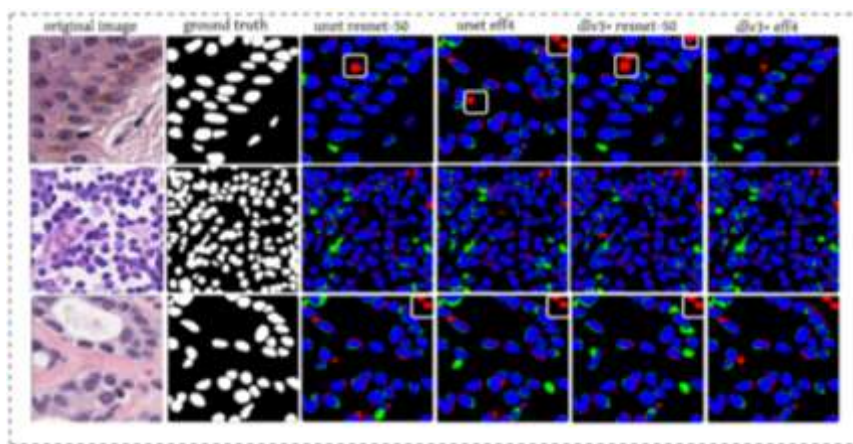


Figure 11. Examples of cell nuclei segmentation by the models, where blue corresponds to correct segments, red to extra pixels, and green to missing pixels in addition to areas of critical regions highlighted by white squares

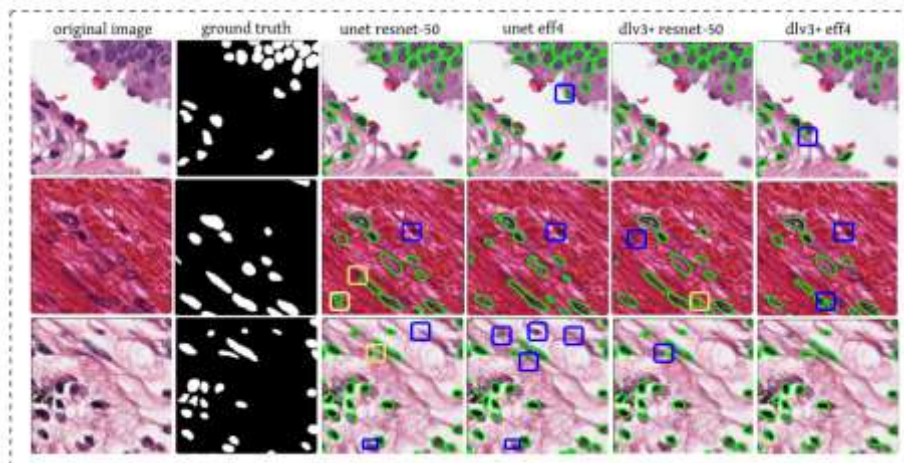


Figure 12. Examples of cell nuclei contours by models in images, where yellow squares indicate errors and blue missing segments

Analysis of IOU values in training, validation, and test sets. In the training phase, the DLV3+ ResNet50 model leads with an IOU score of 90%. In the test set, the models differ further and DLV3+ ResNet50 again leads with 72.80%, followed by U-Net ResNet50 and U-Net eff4 with 71.21% and 71.11%. DLV3+ eff4 shows a significant performance drop in the test set with an IOU of 48.93%, suggesting that the degree of generalization is low on the unfamiliar set, and further tuning is required. The observed performance degradation of DLV3+ eff4, especially during the testing phase, highlights potential problems with its ability to generalize, which is very important for practical applications. Improvements to the model architecture or training procedures, such as integrating regularization strategies or adjusting hyperparameters, can mitigate this overfitting problem.

In Figure 15, when training U-Net ResNet50 and DLV3+ eff4 achieve high accuracy reaching 98%. The U-Net eff4 is slightly in the lead with an accuracy of 95%, while the other models are almost keeping pace. On the test set, U-Net ResNet50 and U-Net eff4 show comparably high accuracies of 94.74% and 94.58% respectively, while DLV3+ ResNet50 also performs strongly at 94.55%. However, the accuracy of DLV3+ eff4 decreases notably to 91.66% in the test evaluation, indicating a decrease in its generalization ability compared to the other models. In summary, DLV3+ ResNet50 and U-Net ResNet50 emerge as top performers, with DLV3+ ResNet50 showcasing percentage in DCS and IOU metrics, and U-Net ResNet50 leading in Acc. This comparative analysis reveals that while DLV3+ eff4 initially demonstrates high training accuracy, its significant drop in performance on the test set points to a limitation in its ability to generalize under varied or unseen conditions.

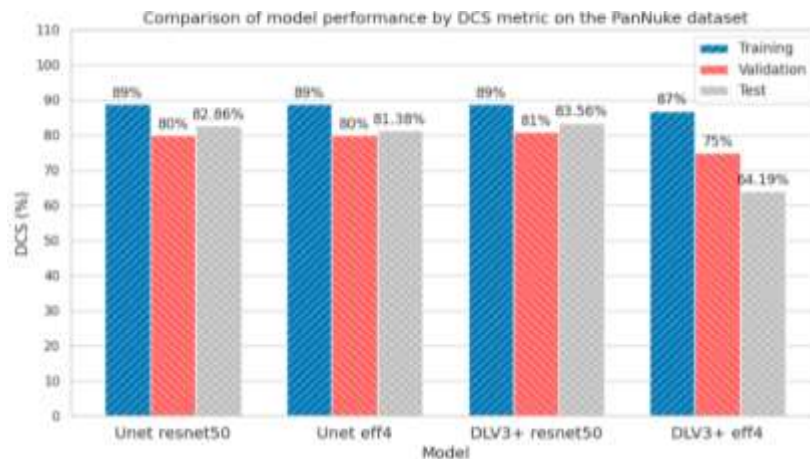


Figure 13. Comparison of performance evaluation of all models by DCS metric

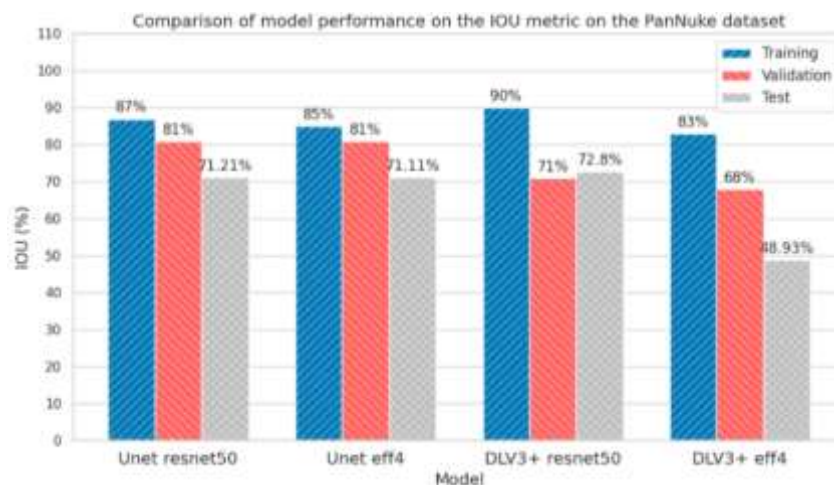


Figure 14. Comparison of performance evaluation of all models by IOU metric

Through research and experimental studies, the authors concluded that convolutional layers with the added ASPP block, with the pre-trained ResNet-50 model, performed better than the other models for segmenting nuclei on a histological dataset for relatively short training and inference times. The introduction of the ASPP block into the Deeplabv3+ network architecture allows for more efficient capture of contextual information at different scales, which holds promise for the development of a system for nuclei segmentation in the future, however, despite the encouraging results, the study highlights the need for further analysis under the influence of different noise levels as well as testing on different color variations [56]. Regularization techniques such as dropout and L2 regularization were applied to prevent overfitting. According to [57], [58], the integration of ASPPs and the use of pre-trained models, in particular ResNet-50, can improve medical segmentation tasks through efficient contextual information gathering and knowledge

transfer. Research on medical nuclei segmentation using computer models shows great promise, but it also faces significant challenges. The main challenges include the difficulty of models to perform equally well on different types of data, the need for large amounts of computing power to train and use them, the difficulty in explaining how the model arrived at its solution, and sensitivity to changes in image quality such as noise or color. All of this indicates that scientists still have a lot of work to do to make these models more accurate, accessible, and understandable for use in real medical practice.

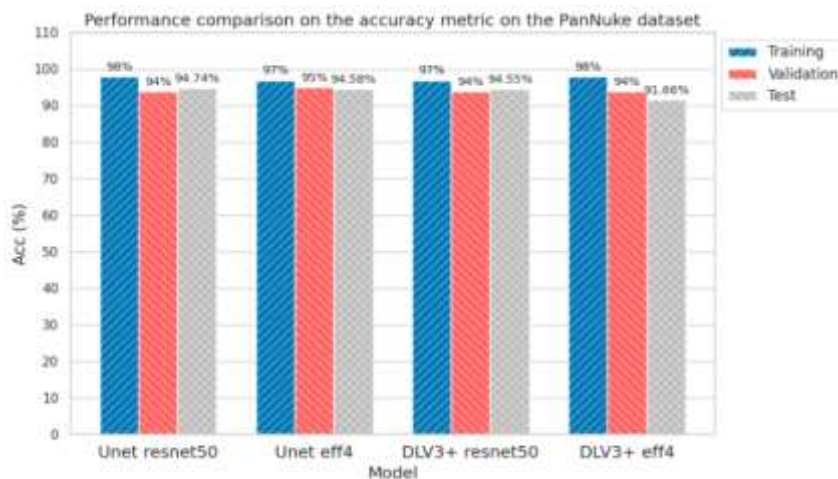


Figure 15. Comparison of performance evaluation of all models by Acc metric

5. CONCLUSION

Concluding the comparison between ResNet50 and EfficientNetB4-based U-Net and DeepLabV3+ models for kernel segmentation on the PanNuke dataset, it can be noted that the ResNet50-based DeepLabV3+ model showed superior performance, achieving a dice similarity score (DCS) of 0.8356 and an IOU of 0.7280. This high level of performance can be attributed to the application of a robust dropout coefficient of 0.7 and L2 regularization at 0.02. Given these results, future research should aim at extending the scope of application of the efficient ResNet50-based DeepLabV3+ model beyond its current domain. This includes applying the model to different modalities of medical imaging to evaluate its performance and versatility in different diagnostic scenarios. Future research should explore the model's potential in the early detection of diseases, which may be crucial for patient care. Future studies may also benefit from incorporating cross-validation with a wider range of datasets to confirm the reliability and adaptability of the model. Exploring transfer learning to adapt a pre-trained model on PanNuke datasets to other types of histopathology data, including rare diseases, may provide insight into the generalizability of the model.

REFERENCES





- [1] E. G. Fischer, "Nuclear morphology and the biology of cancer cells," *Acta Cytologica*, vol. 64, no. 6, pp. 511–519, 2020, doi: 10.1159/000508780.
- [2] C. Frick *et al.*, "Quantitative estimates of preventable and treatable deaths from 36 cancers worldwide: a population-based study," *The Lancet Global Health*, vol. 11, no. 11, pp. e1700–e1712, Nov. 2023, doi: 10.1016/S2214-109X(23)00406-0.
- [3] K. Umurzakov, D. Kaidarova, B. Apsalikov, and G. Shalgumbayeva, "Kidney cancer epidemiology in Kazakhstan, 2010–2019," *Oncologia i radiologia Kazakhstana*, vol. 58, no. 4, pp. 12–17, Dec. 2020, doi: 10.52532/2663-4864-2020-4-58-12-17.
- [4] M. Kowal, M. Żejmo, M. Skobel, J. Korbicz, and R. Monczak, "Cell nuclei segmentation in cytological images using convolutional neural network and seeded watershed algorithm," *Journal of Digital Imaging*, vol. 33, no. 1, pp. 231–242, Feb. 2020, doi: 10.1007/s10278-019-00200-8.
- [5] S. Singh, V. Bhateja, S. Gupta, S. Verma, S. Urooj, and D.-N. Le, "Nucleus segmentation using k-means clustering for analysis of microscopy images," in *Advances in Intelligent Systems and Computing*, 2023, pp. 105–113.
- [6] J. Ma, Y. A. Muad, and J. Chen, "Visualization of medical volume data based on improved K-means clustering and segmentation rules," *IEEE Access*, vol. 9, pp. 100498–100512, 2021, doi: 10.1109/ACCESS.2021.3096790.
- [7] T. Luo, Y. Lu, S. Liu, D. Lin, and J. Qu, "Enhanced visualization of hematoxylin and eosin stained pathological characteristics by phasor approach," *Analytical Chemistry*, vol. 89, no. 17, pp. 9224–9231, Sep. 2017, doi: 10.1021/acs.analchem.7b01999.
- [8] H. Irshad, A. Veillard, L. Roux, and D. Racocanu, "Methods for nuclei detection, segmentation, and classification in digital histopathology: A review-current status and future potential," *IEEE Reviews in Biomedical Engineering*, vol. 7, pp. 97–114, 2014, doi: 10.1109/RBME.2013.2295804.
- [9] L. Alzubaidi *et al.*, "Review of deep learning: concepts, CNN architectures, challenges, applications, future directions," *Journal of Big Data*, vol. 8, no. 1, p. 53, Mar. 2021, doi: 10.1186/s40537-021-00444-8.

- [10] Z. Li, F. Liu, W. Yang, S. Peng, and J. Zhou, "A survey of convolutional neural networks: analysis, applications, and prospects," *IEEE Transactions on Neural Networks and Learning Systems*, vol. 33, no. 12, pp. 6999–7019, Dec. 2022, doi: 10.1109/TNNLS.2021.3084827.
- [11] W. Gómez-Flores and W. Coelho de Albuquerque Pereira, "A comparative study of pre-trained convolutional neural networks for semantic segmentation of breast tumors in ultrasound," *Computers in Biology and Medicine*, vol. 126, p. 104036, Nov. 2020, doi: 10.1016/j.combiomed.2020.104036.
- [12] D. Karimi, S. D. Vasylychko, and A. Gholipour, "Convolution-Free Medical Image Segmentation Using Transformers," *Lecture Notes in Computer Science (including subseries Lecture Notes in Artificial Intelligence and Lecture Notes in Bioinformatics)*, vol. 12901 LNCS, pp. 78–88, 2021, doi: 10.1007/978-3-030-87193-2_8.
- [13] J. E. Ball, D. T. Anderson, and C. S. Chan, "Comprehensive survey of deep learning in remote sensing: theories, tools, and challenges for the community," *Journal of Applied Remote Sensing*, vol. 11, no. 04, p. 1, Sep. 2017, doi: 10.1117/1.jrs.11.042609.
- [14] C. Wei, S. Kakade, and T. Ma, "The implicit and explicit regularization effects of dropout," *37th International Conference on Machine Learning, ICML 2020*, vol. PartF16814, pp. 10112–10123, 2020.
- [15] K. Al-Dulaimi, J. Banks, K. Nugyen, A. Al-Sabaawi, I. Tomeo-Reyes, and V. Chandran, "Segmentation of white blood cell, nucleus and cytoplasm in digital haematology microscope images: a review-challenges, current and future potential techniques," *IEEE Reviews in Biomedical Engineering*, vol. 14, pp. 290–306, 2021, doi: 10.1109/RBME.2020.3004639.
- [16] D. R. Sarvamangala and R. V. Kulkarni, "Convolutional neural networks in medical image understanding: a survey," *Evolutionary Intelligence*, vol. 15, no. 1, pp. 1–22, Mar. 2022, doi: 10.1007/s12065-020-00540-3.
- [17] H. Yu, L. T. Yang, Q. Zhang, D. Armstrong, and M. J. Deen, "Convolutional neural networks for medical image analysis: state-of-the-art, comparisons, improvement and perspectives," *Neurocomputing*, vol. 444, pp. 92–110, Jul. 2021, doi: 10.1016/j.neucom.2020.04.157.
- [18] O. Ronneberger, P. Fischer, and T. Brox, "U-Net: convolutional networks for biomedical image segmentation," in *Lecture Notes in Computer Science (including subseries Lecture Notes in Artificial Intelligence and Lecture Notes in Bioinformatics)*, vol. 9351, 2015, pp. 234–241.
- [19] L. Liu, J. Cheng, Q. Quan, F. X. Wu, Y. P. Wang, and J. Wang, "A survey on U-shaped networks in medical image segmentations," *Neurocomputing*, vol. 409, pp. 244–258, Oct. 2020, doi: 10.1016/j.neucom.2020.05.070.
- [20] A. Al Qurri and M. Almekkawy, "Improved U-Net with attention for medical image segmentation," *Sensors (Basel, Switzerland)*, vol. 23, no. 20, p. 8589, Oct. 2023, doi: 10.3390/s23208589.
- [21] J. Wang, X. Zhang, P. Lv, H. Wang, and Y. Cheng, "Automatic liver segmentation using EfficientNet and attention-based residual U-Net in CT," *Journal of Digital Imaging*, vol. 35, no. 6, pp. 1479–1493, Dec. 2022, doi: 10.1007/s10278-022-00668-x.
- [22] X. Li, Y. Wang, Q. Tang, Z. Fan, and J. Yu, "Dual U-Net for the segmentation of overlapping glioma nuclei," *IEEE Access*, vol. 7, pp. 84040–84052, 2019, doi: 10.1109/ACCESS.2019.2924744.
- [23] J. Li and X. Li, "MIU-Net: MIX-attention and inception U-Net for histopathology image nuclei segmentation," *Applied Sciences (Switzerland)*, vol. 13, no. 8, p. 4842, Apr. 2023, doi: 10.3390/app13084842.
- [24] R. I. Sumon *et al.*, "Densely convolutional spatial attention network for nuclei segmentation of histological images for computational pathology," *Frontiers in Oncology*, vol. 13, May 2023, doi: 10.3389/fonc.2023.1009681.
- [25] S. Lal, D. Das, K. Alabhya, A. Kanfode, A. Kumar, and J. Kini, "NucleiSegNet: Robust deep learning architecture for the nuclei segmentation of liver cancer histopathology images," *Computers in Biology and Medicine*, vol. 128, p. 104075, Jan. 2021, doi: 10.1016/j.combiomed.2020.104075.
- [26] Y. Zhou, O. F. Onder, Q. Dou, E. Tsougenis, H. Chen, and P. A. Heng, "CIA-Net: robust nuclei instance segmentation with contour-aware information aggregation," in *Lecture Notes in Computer Science (including subseries Lecture Notes in Artificial Intelligence and Lecture Notes in Bioinformatics)*, vol. 11492 LNCS, 2019, pp. 682–693.
- [27] M. M. Kalayeh and M. Shah, "On symbiosis of attribute prediction and semantic segmentation," *IEEE Transactions on Pattern Analysis and Machine Intelligence*, vol. 43, no. 5, pp. 1620–1635, 2021, doi: 10.1109/TPAMI.2019.2956039.
- [28] T. D. Le, S. G. Kwon, S.-H. Lee, K.-R. Kwon, T. Le Dinh, and S.-G. Kwon, "Breast Tumor Cell Nuclei Segmentation in Histopathology Images using EfficientUnet++ and Multi-organ Transfer Learning," *Article in Journal of Korea Multimedia Society*, vol. 24, no. 8, pp. 1000–1011, 2021, doi: 10.9717/kjms.2021.24.8.1000.
- [29] Z. Zhou, M. M. R. Siddiquee, N. Tajbakhsh, and J. Liang, "Unet++: a nested u-net architecture for medical image segmentation," in *Lecture Notes in Computer Science (including subseries Lecture Notes in Artificial Intelligence and Lecture Notes in Bioinformatics)*, vol. 11045 LNCS, 2018, pp. 3–11.
- [30] M. Tan and Q. V. Le, "EfficientNet: rethinking model scaling for convolutional neural networks," *36th International Conference on Machine Learning, ICML 2019*, vol. 2019-June, pp. 10691–10700, 2019.
- [31] T. W. Cenggoro, "Incorporating the knowledge distillation to improve the EfficientNet transfer learning capability," in *2020 International Conference on Data Science and Its Applications (ICoDSA)*, Aug. 2020, pp. 1–5, doi: 10.1109/ICoDSA50139.2020.9212994.
- [32] Y. Lu, X. Qin, H. Fan, T. Lai, and Z. Li, "WBC-Net: a white blood cell segmentation network based on UNet++ and ResNet," *Applied Soft Computing*, vol. 101, p. 107006, Mar. 2021, doi: 10.1016/j.asoc.2020.107006.
- [33] C. Si, W. Yu, P. Zhou, Y. Zhou, X. Wang, and S. Yan, "Inception transformer," *Advances in Neural Information Processing Systems*, vol. 35, May 2022, [Online]. Available: <http://arxiv.org/abs/2205.12956>.
- [34] Y. Zhu and S. Newsam, "DenseNet for dense flow," in *Proceedings - International Conference on Image Processing, ICIP*, Sep. 2017, vol. 2017-Sept, pp. 790–794, doi: 10.1109/ICIP.2017.8296389.
- [35] A. Younis, L. Qiang, C. O. Nyatega, M. J. Adamu, and H. B. Kawuwa, "Brain tumor analysis using deep learning and VGG-16 ensembling learning approaches," *Applied Sciences (Switzerland)*, vol. 12, no. 14, p. 7282, Jul. 2022, doi: 10.3390/app12147282.
- [36] A. Mukasheva, D. Koishiyeva, Z. Suimenbayeva, S. Rakhmetulayeva, A. Bolshibayeva, and G. Sadikova, "Comparison evaluation of unet-based models with noise augmentation for breast cancer segmentation on ultrasound image," *Eastern-European Journal of Enterprise Technologies*, vol. 5, no. 9 (125), pp. 85–97, Oct. 2023, doi: 10.15587/1729-4061.2023.289044.
- [37] S. Belharbi, "Neural networks regularization through representation learning," *arXiv*, Jul. 2018, [Online]. Available: <http://arxiv.org/abs/1807.05292>.
- [38] S. Lefkovits and L. Lefkovits, "U-Net architecture variants for brain tumor segmentation of histogram corrected images," *Acta Universitatis Sapientiae, Informatica*, vol. 14, no. 1, pp. 49–74, Aug. 2022, doi: 10.2478/ausi-2022-0004.
- [39] W. Liu, J. Luo, Y. Yang, W. Wang, J. Deng, and L. Yu, "Automatic lung segmentation in chest X-ray images using improved U-Net," *Scientific Reports*, vol. 12, no. 1, p. 8649, May 2022, doi: 10.1038/s41598-022-12743-y.





- [40] L. Kou, M. Sysyn, S. Fischer, J. Liu, and O. Nabochenko, "Optical rail surface crack detection method based on semantic segmentation replacement for magnetic particle inspection," *Sensors*, vol. 22, no. 21, p. 8214, Oct. 2022, doi: 10.3390/s22218214.
- [41] J. Zhang, H. Hu, T. Yang, Q. Hu, Y. Yu, and Q. Huang, "HR-ASPP: An improved semantic segmentation model of cervical nucleus images with accurate spatial localization and better shape feature extraction based on Deeplabv3+," in *Proceedings of the 15th International Conference on Digital Image Processing*, May 2023, pp. 1–8, doi: 10.1145/3604078.3604094.
- [42] J. Deng, W. Dong, R. Socher, L.-J. Li, Kai Li, and Li Fei-Fei, "ImageNet: a large-scale hierarchical image database," in *2009 IEEE Conference on Computer Vision and Pattern Recognition*, Jun. 2010, pp. 248–255, doi: 10.1109/cvpr.2009.5206848.
- [43] S. Santurkar, D. Tsipras, A. Ilyas, and A. Madry, "How does batch normalization help optimization?," *Advances in Neural Information Processing Systems*, vol. 2018-Decem, pp. 2483–2493, 2018, doi: 10.48550/arXiv.1805.11604.
- [44] H. Ide and T. Kurita, "Improvement of learning for CNN with ReLU activation by sparse regularization," in *Proceedings of the International Joint Conference on Neural Networks*, May 2017, vol. 2017-May, doi: 10.1109/IJCNN.2017.7966185.
- [45] A. Lewkowycz and G. Gur-Ari, "On the training dynamics of deep networks with L2 regularization," *Advances in Neural Information Processing Systems*, vol. 2020-Decem, 2020.
- [46] Y. Assiri, "Stochastic optimization of plain convolutional neural networks with Simple methods," *arXiv*, 2020, [Online]. Available: <http://arxiv.org/abs/2001.08856>.
- [47] X. Lian, Y. Pang, J. Han, and J. Pan, "Cascaded hierarchical atrous spatial pyramid pooling module for semantic segmentation," *Pattern Recognition*, vol. 110, p. 107622, Feb. 2021, doi: 10.1016/j.patcog.2020.107622.
- [48] J. Gamper, N. A. Koohbanani, K. Benet, A. Khuram, and N. Rajpoot, "PanNuke: an open pan-cancer histology dataset for nuclei instance segmentation and classification," in *Lecture Notes in Computer Science (including subseries Lecture Notes in Artificial Intelligence and Lecture Notes in Bioinformatics)*, vol. 11435 LNCS, 2019, pp. 11–19.
- [49] M. Yeung, E. Sala, C. B. Schönlieb, and L. Rundo, "Unified focal loss: generalising dice and cross entropy-based losses to handle class imbalanced medical image segmentation," *Computerized Medical Imaging and Graphics*, vol. 95, p. 102026, Jan. 2022, doi: 10.1016/j.compmedimag.2021.102026.
- [50] A. Iqbal, M. Sharif, M. A. Khan, W. Nisar, and M. Alhaisoni, "FF-UNet: a U-Shaped deep convolutional neural network for multimodal biomedical image segmentation," *Cognitive Computation*, vol. 14, no. 4, pp. 1287–1302, Jul. 2022, doi: 10.1007/s12559-022-10038-y.
- [51] A. Mukasheva, Z. Akanov, and D. Yedilkhan, "Research of the regression analysis methods for predicting the growth of patients with diabetes mellitus," in *SIST 2021 - 2021 IEEE International Conference on Smart Information Systems and Technologies*, Apr. 2021, pp. 1–7, doi: 10.1109/SIST50301.2021.9465975.
- [52] Y. A. Ayalew, K. A. Fante, and M. A. Mohammed, "Modified U-Net for liver cancer segmentation from computed tomography images with a new class balancing method," *BMC Biomedical Engineering*, vol. 3, no. 1, p. 4, Dec. 2021, doi: 10.1186/s42490-021-00050-y.
- [53] E. Bisong, *Building machine learning and deep learning models on google cloud platform*. Berkeley, CA: Apress, 2019.
- [54] S. Markidis, S. W. D. Chien, E. Laure, I. B. Peng, and J. S. Vetter, "NVIDIA tensor core programmability, performance & precision," in *Proceedings - 2018 IEEE 32nd International Parallel and Distributed Processing Symposium Workshops, IPDPSW 2018*, May 2018, pp. 522–531, doi: 10.1109/IPDPSW.2018.00091.
- [55] B. Pang, E. Nijkamp, and Y. N. Wu, "Deep learning with TensorFlow: a review," *Journal of Educational and Behavioral Statistics*, vol. 45, no. 2, pp. 227–248, Apr. 2020, doi: 10.3102/1076998619872761.
- [56] A. Mukasheva, S. Rakhmetulayeva, G. Astabayeva, and S. Gnatyuk, "Developing a system for diagnosing diabetes mellitus using bigdata," *Eastern-European Journal of Enterprise Technologies*, vol. 5, no. 2–119, pp. 75–85, Oct. 2022, doi: 10.15587/1729-4061.2022.266185.
- [57] W. Song, H. Yu, and J. Wu, "PLU-Net: extraction of multiscale feature fusion," *Medical Physics*, vol. 51, no. 4, pp. 2733–2740, Apr. 2024, doi: 10.1002/mp.16840.
- [58] P. Guo, X. Su, H. Zhang, M. Wang, and F. Bao, "A multi-scaled receptive field learning approach for medical image segmentation," in *ICASSP, IEEE International Conference on Acoustics, Speech and Signal Processing - Proceedings*, May 2020, vol. 2020-May, pp. 1414–1418, doi: 10.1109/ICASSP40776.2020.9054030.

BIOGRAPHIES OF AUTHORS







Dina Koishiyeva     is a graduate from the Faculty of Radio Engineering, Electronics, and Telecommunications in 2016, is currently pursuing her Master's in Information Systems at Almaty University of Energy and Telecommunications. Her focus encompasses machine learning, neural networks, AI, and medical image segmentation. With interests spanning machine intelligence and image processing, Dina excels in data mining and statistical learning. For inquiries or collaborations. She can be contacted at email: dina290692@gmail.com.







Madina Sydybayeva     doctoral student at the International University of Information Technologies, Almaty. In 1994, she received a diploma in the specialty "Computer complexes, systems and networks" from the Kazakh National Technical University. K.I. Satpayeva. In 2012, she received a diploma in "automation and control" from the Kazakh National Agrarian University. She is the author of more than 40 publications. Her research interests include the area of modern network technologies in scientific research. She can be contacted by email: madinasydybayeva@gmail.com.







Saule Belginova     received the Master of Engineering academic degree of specialty “Mathematical and computer modeling” and the Ph.D. degree of specialty Information Systems from D. Serikbayev East Kazakhstan State Technical University (EKSTU), Oskemen, Kazakhstan, in 2014 and 2020, respectively. At the present she is an associate professor of Information Technology department in University “Turan”, Almaty, Kazakhstan. She has authored or coauthored more than 40 publications. Her research interests include mathematical and computer modeling of processes, intellectual analysis of medical data. She can be contacted at email: sbelginova@gmail.com.







Damelya Yeskendirowa     is Candidate of Technical Sciences, Assistant Professor of International Information Technologies University, Almaty. She received a diploma in Computer Science and Management in 1998 from Aktau State University named after Sh. Yesenova. She defended her Ph.D. thesis on the topic “Models and methods of synthesis of dynamic frequency-pulse automatic control systems” in 2010 and received the degree of Candidate of Technical Sciences. She is the author of more than 60 publications. Her research interests include the field of artificial intelligence, educational issues, and data mining. She can be contacted at email: zerek.2023@gmail.com.







Zhanerke Azamatova     received candidate of Technical Sciences in the specialty “Automation and control” dissertation Council By 14.29.15 EKSTU named after D. Serikbayev. I am an acting associate professor since 2020 of the School of Metallurgy and Mineral Processing of the D. Serikbayev National Technical University. Author of more than 15 publications. Her research interests include the field of automation and control. She can be contacted at email: Zhanerkez@mail.ru.



Azamat Kalpebayev     he received an academic master's degree in information systems in the specialty “Information Systems” at the Kazakh National Technical University named after K. Satbayev (KazNTU), Almaty, Kazakhstan, in 2003. Currently, he works as a senior lecturer at the Department of IT Engineering of the Almaty University of Energy and Communications named after G. Daukeev, Almaty, Kazakhstan. He is the author or co-author of more than 5 publications. His research interests include big data, mathematical and computer modeling of business processes, and integration of artificial intelligence. He can be contacted at email: azamat.kalpe@gmail.com.



Gulzhanat Beketova     Ph.D., associate professor in 2017, she completed a full course of doctoral studies in specialty 6D070400 – Computer technology and software and defended her doctoral dissertation. She works as an associate professor at the Department of IT Engineering of the Almaty University of Energy and Communications named after G. Daukeev, Almaty, Kazakhstan. The total number of published scientific and methodological works is more than 60, of which more than 3 are in the bibliographic databases Scopus, Elsevier, Web of Science, 2 are scientific manuals, 1 is a monograph. There are also many certificates of state registration of rights to an object of copyright by the Ministry of Justice of the Republic of Kazakhstan. She can be contacted at email: beketova_gs@mail.ru.